Miranda, E.A., et al., 2023, Making sense of shear zone fabrics that record multiple episodes of deformation: Electron backscatter diffraction–derived and crystallographic vorticity axis–enhanced petrochronology: Geology, https://doi.org/10.1130/G50982.1.

Supplemental Material

Text:

1. EBSD Methods and Working Conditions and Supplemental Table 1
2. LA-SF-ICPMS U-Pb Titanite Petrochronology Methods
3. U-Pb titanite data Supplementary Tables 2 and 3 (separate Excel file)
4. EDS maps and photomicrographs of titanite clusters in Large Pluton samples
5. Sample locations and fabric orientation data
6. Photomicrographs and EBSD maps of Misty Pluton and Large Pluton samples

Excel file:

Supplemental Table 2. U-Pb isotope data.
Supplemental Table 3. U-Pb isotope data for standards
DRS Settings

Supplemental Material

Contents:

1. EBSD Methods and Working Conditions

EBSD map data were collected using a ThermoScientific Apreo Field Emission Scanning Electron Microscope (SEM) with an Oxford Instruments Symmetry EBSD detector and Aztec software, located at UC San Diego within the Nanoengineering Materials Research Center; all SEM operating conditions for each sample can be found below. Beam currents and spot sizes are reported together; beam currents of 26 and 51 nA correspond to the unitless spot size values of 16 and 17, respectively.

Sample	**Accelerating Voltage**	**Beam Current (nA)**	**Spot Size (unitless, unique to microscope)**	**EBSD Map Step Size**	**Working Distance**
19MP14	20 kV	26-51	16-17	5 um	25 mm
19MP19	20 kV	26-51	16-17	7.5 um	25 mm
19MP23	20 kV	26-51	16-17	7.5 um	25 mm
19MT03	20 kV	26-51	16-17	10 um	25 mm
19MT13	20 kV	26-51	16-17	10 um	25 mm
19MT09	20 kV	26-51	16-17	10 um	25 mm

Supplementary Table 1. *SEM operating conditions used when setting up EBSD large area maps for all samples.*

After being collected via Aztec, our EBSD data were exported using the HKL Channel 5 software suite by Oxford Instruments and saved to be directly imported into MATLAB. Within MATLAB, we used the MTEX toolbox version 5.7.0 to process our data to ultimately produce EBSD phase and orientation maps for each sample. In MTEX, we define grain boundaries as having $\geq$ 10° of misorientation relative to other grains, and we define low-angle boundaries as those having 2-10° of misorientation; these classifications also helped to determine grain counts for each phase. The maps were minimally post-processed in MTEX; we removed wild spikes (1 pixel "grains") and small grains, which are defined as being < 10 pixels in area.

We also used the MTEX toolbox 5.7.0 to plot crystallographic preferred orientations (CPOs) and crystallographic vorticity axis (CVA) data. CVA analysis uses intragranular orientations determined by EBSD to calculate a dispersion, or vorticity, axis for a mineral grain (Michels et al., 2015). The dispersion axes for individual mineral grains were then plotted on contoured lower-hemisphere equal-area stereographic projections to show: 1) a bulk vorticity for the entire sample, and 2) the vorticity axis for each mineral phase. In order to plot CVA figures for the bulk rock and for individual mineral phases, we used the open-source code on GitHub (https://github.com/zmichels/CVA).

2. LA-SF-ICPMS U-Pb Titanite Petrochronology

U-Pb petrochronology of titanite grains was conducted using laser-ablation of titanite in thin sections. Before laser ablation of titanite, we performed EBSD and EDS analysis of individual titanite grains to image any microstructures/crystal-lattice distortions and rim/core relationships. We used CSUN's FEI Quanta 600 SEM to collect 1) backscattered electron images (BSEs), 2) EBSD Mis2Mean maps for misorientation analysis, and 3) EDS maps to investigate elemental distributions within individual grains. EDS maps were created to specifically index for

the following elements based on methods from Moser et al. (2022): Na, Mg, K, Ca, Ti, Zr, Nb, Ce, Fe, Al, Si, P, S, and O.

Uranium-lead ratios and trace element abundances were collected using a ThermoScientific Element2 SF-ICPMS coupled with a Teledyne Cetec Analyte G2 Excimer Laser (operating at a wavelength of 193 nm) at California State University Northridge. Prior to analysis the Element2 was tuned using the NIST 612 glass standard to optimize signal intensity and stability. Laser beam diameter was ~35 microns at 10 Hz and 80% power. Ablation was performed in a HelEx II Active 2-Volume Cellä and sample aerosol was transported with He carrier gas through Teflon-lined tubing, where it was mixed with Ar gas before introduction to the plasma torch. Flow rates for Ar and He gases were as follows: Ar cooling gas (16.0 NL/min), Ar auxiliary gas (1.0 NL/min), He carrier gas (~0.3-0.5 NL/min), Ar sample gas (1.1-1.3 NL/min). Isotope data were collected in E-scan mode with magnet set at mass 202, and RF Power at 1245 W. Isotopes measured include ^{91Z}r, ^{139}La, ^{146}Nd, ^{152}Sm, ^{163}Dy, ^{172}Yb, ^{202}Hg, ^{204}(Pb+Hg), ^{206}Pb, ^{207}Pb, ^{208}Pb, ^{232}Th, and ^{238}U. All isotopes were collected in counting mode with the exception of ^{232}Th and ^{238}U which were collected in analogue mode. Analyses were conducted in a ~40-minute time resolved analysis mode. Each analysis consisted of a 30-second integration with the laser firing on sample, and a 20 second delay to purge the previous sample and move to the next sample. Approximate depth of the ablation pit was ~20-30 microns.

The primary age standard, MKED, was analyzed every 10 analyses to correct for in-run fractionation of Pb/U and Pb isotopes. A secondary standard consisting of Fish Canyon Tuff titanites (Lanphere et al., 2001; Kuiper et al., 2008) were analyzed every ~10 analyses to assess reproducibility of the data. Depending on abundance, between 30-50 titanite grains per sample were picked from polished thin sections and analyzed. Data were reduced with Iolite (Paton et

al., 2010). Titanite data presented in this study are corrected for common Pb using a regression on the Tera-Wasserburg Pb/U isochron, where the y-intercept will yield the $^{207}Pb/^{206}Pb$ isotopic ratio of the common Pb for each individual sample (Storey et al., 2006). Titanite ages are presented as lower intercepts calculated from regression of $^{207}Pb/^{206}Pb$ and $^{238}U/^{206}Pb$ data by IsoplotR (Vermeesch, 2018). Quoted titanite dates in Supplementary Tables 2-3 are reported with 2SE internal uncertainties, whereas lower intercept ages are assigned 2% total uncertainties based on reproducibility of standards during analyses. In this study, U-Pb analysis of Fish Canyon tuff titanites yielded a lower intercept of 27.0 ± 1.8 Ma (n=26) (MSWD = 1.1) which is within close agreement of the accepted ages of 28.201 ± 0.012 Ma (Lanphere et al., 2001; Kuiper et al., 2008).

3. U-Pb titanite data Supplementary Tables 2 and 3 (Excel file)

Titanite U-Pb data are included in Supplementary Table 2. The standards are reported in Supplementary Table 3 along with data reduction parameters. Both tables are worksheet tabs within an Excel file that can be downloaded separately.

4. EDS Maps and Photomicrographs of Titanite Clusters

Figure SM1. Energy Dispersive Spectroscopy (EDS) maps and photomicrographs of titanite clusters in Large Pluton Samples 19MP19 and 19MP23. A) EDS Maps of Ti, Ca, Ce, and Nb for titanites in 19MP19 and 19MP23. Laser spots are labeled with temperatures calculated by Zr-in-titanite thermometry. B) Photomicrograph of titanite clusters in Sample 19MP19 in cross polarized light. White dashed line shows approximate trace of foliation. White rectangle shows location of inset photo in plane light (below) showing titanite grains with laser holes from LA-

ICPMS analysis. C) Photomicrograph of titanite clusters in Sample 19MP23 in cross polarized light. White dashed line shows approximate trace of foliation. White rectangle shows location of inset photo in plane light (below) showing titanite grains with laser holes from LA-ICPMS analysis.

5. Sample locations and fabric orientation data

Sample	Northing	Easting	Lat	Long	Altitude (m)	Foliation Orientation (Strike/Dip)	Lineation Orientation (Plunge/Trend)
19MP14	4995295	1155662	-45.05618	167.35675	1039.8	165, 79 SW	15/182
19MP19	4995769	1155870	-45.05206	167.3598	1212.2	005, 75 E	47/182
19MP23	4996035	1156591	-45.05013	167.36914	1075.5	235, 60 NW	50/224
19MT03	4987599	1155387	-45.12494	167.34645	866.8	057, 24 SE	15/210
19MT13	4987669	1155721	-45.12453	167.35074	771	018, 89 E	19/205
19MT09	4987733	1156368	-45.12436	167.35898	963.5	250, 33 NW	none
	NZ Transverse Mercator		WGS84				

6. Photomicrographs and EBSD Maps of Misty Pluton and Large Pluton samples

Figure SM2. Misty Pluton Sample 19MT03

Figure SM3. Misty Pluton Sample 19MT13

Figure SM4. Misty Pluton Sample 19MT09

Figure SM5. Large Pluton Sample 19MP19

Figure SM6. Large Pluton Sample 19MP23

Figure SM2. Photomicrographs and EBSD phase map for Misty Pluton Sample 19MT03. A) Whole thin section photomicrograph in cross polarized light. Larger white rectangle shows

location of EBSD map shown in Figure SM2c. B) Photomicrograph of plagioclase subgrain rotation recrystallization (SGR) dynamic recrystallization microstructures and plagioclase deformation twinning. Plag: plagioclase Ep: epidote. C) EBSD phase map of inset region of Figure SM2a.

Figure SM3. Photomicrographs and EBSD phase map for Misty Pluton Sample 19MT13. A) Whole thin section photomicrograph in cross polarized light. Large white rectangle shows location of EBSD map shown in Figure SM3c. B) Photomicrograph of plagioclase subgrain rotation recrystallization (SGR) dynamic recrystallization microstructures and plagioclase deformation twinning. Plag: plagioclase; Hbl: hornblende; Ep: epidote. C) EBSD phase map of inset region of Figure SM3a.

Figure SM4. Photomicrographs and EBSD phase map for Misty Pluton Sample 19MT09. A) Whole thin section photomicrograph in cross polarized light. Largest white rectangle shows location of EBSD map shown in Figure SM4d. B) Photomicrograph of sinuous plagioclase grain boundaries, indicative of grain boundary mobility during recrystallization. Plag: plagioclase; Hbl: hornblende; Ep: epidote. C) Photomicrograph of subgrain development in plagioclase (Plag). D) EBSD phase map of inset region of Figure SM4a.

Figure SM5. Photomicrographs and EBSD phase map for titanite-bearing Large Pluton Sample 19MP19. A) Whole thin section photomicrograph in cross polarized light. Largest white rectangle shows location of EBSD map shown in Figure SM5e. B) Photomicrograph of grain boundary migration (GBM) dynamic recrystallization microstructures in quartz (Qtz) and

chessboard extinction patterns in quartz, both of which indicate deformation at temperatures >600ºC. C) Photomicrograph of deformation twinning and cuspate-lobate grain boundaries in plagioclase (Plag), indicating the onset of crystal plasticity in feldspar. D) Photomicrograph of sweeping extinction in biotite (Bt) grain demonstrating crystal-plastic deformation. E) EBSD phase map of inset region of Figure SM5a.

Figure SM6. Photomicrographs and EBSD phase map for titanite-bearing Large Pluton Sample 19MP23. A) Whole thin section photomicrograph in cross polarized light. Largest white rectangle shows location of EBSD map shown in Figure SM6d. Bb) Photomicrograph of grain boundary migration (GBM) dynamic recrystallization microstructures in quartz (Qtz) and deformation twinning in plagioclase (Plag). C) Photomicrograph of grain boundary migration (GBM) dynamic recrystallization microstructures in quartz (Qtz) and deformation twinning and subgrain development in plagioclase (Plag). D) Photomicrograph of coarse, bent muscovite (Musc) grain exhibiting sweeping extinction, indicative of crystal plastic deformation in micas. E) EBSD phase map of inset region of Figure SM6a.

References cited in Supplemental Material

Kirkland, C.L., Fougerouse, D., Reddy, S.M., Hollis, J., and Saxey, D.W., 2018, Assessing the mechanisms of common Pb incorporation into titanite: Chemical Geology, v. 483, p. 558–566, doi:10.1016/J.CHEMGEO.2018.03.026.

Kuiper, K.F., Deino, A., Hilgen, P.J., Krijgsman, W., Renne, P.R., and Wijbrans, J.R., 2008, Synchronizing rock clocks of Earth history. Science, 320, p. 500-504.

Lanphere, M.A. and Baadsraard, H., 2001, Precise K-Ar, 40 Ar/39 Ar, Rb-Sr and U-Pb mineral ages from the 27.5 Ma Fish Canyon Tuff reference standard. Chemical Geology, 175, p. 653-671.

Michels, Z.D., Kruckenberg, S.C., Davis, J.R., &Tikoff, B. (2015). Determining vorticity axes from grain-scale dispersion of crystallographic orientations: Geology, v. 43, p. 803–806

Moser, A. C., Hacker, B. R., Gehrels, G. E., Seward, G. G., Kylander-Clark, A. R., & Garber, J. M. (2022). Linking titanite U–Pb dates to coupled deformation and dissolution-reprecipitation: Contributions to Mineralogy and Petrology, v. 177(3), p. 1-27.

Paton, C., Woodhead, J., Hellstrom, J. Hergt, J., Greig, A., Maas, R., (2010). Improved laser ablation U-Pb zircon geochronology through robust downhole fractionation correction: Geochemistry, Geophysics, Geosystems, 11, 10.1029/2009GC002618

Storey, C.D., Jeffries, T.E., and Smith, M., 2006, Common lead-corrected laser ablation ICP–MS U–Pb systematics and geochronology of titanite: Chemical Geology, v. 227, p. 37–52, doi:10.1016/J.CHEMGEO.2005.09.003.

Vermeesch, P., 2018, IsoplotR: a free and open toolbox for geochronology. Geoscience Frontiers, v.9, p.1479-1493.

Figure SM1. **Energy Dispersive Specroscopy (EDS) Maps and Photomicrographs of Titanite Clusters**

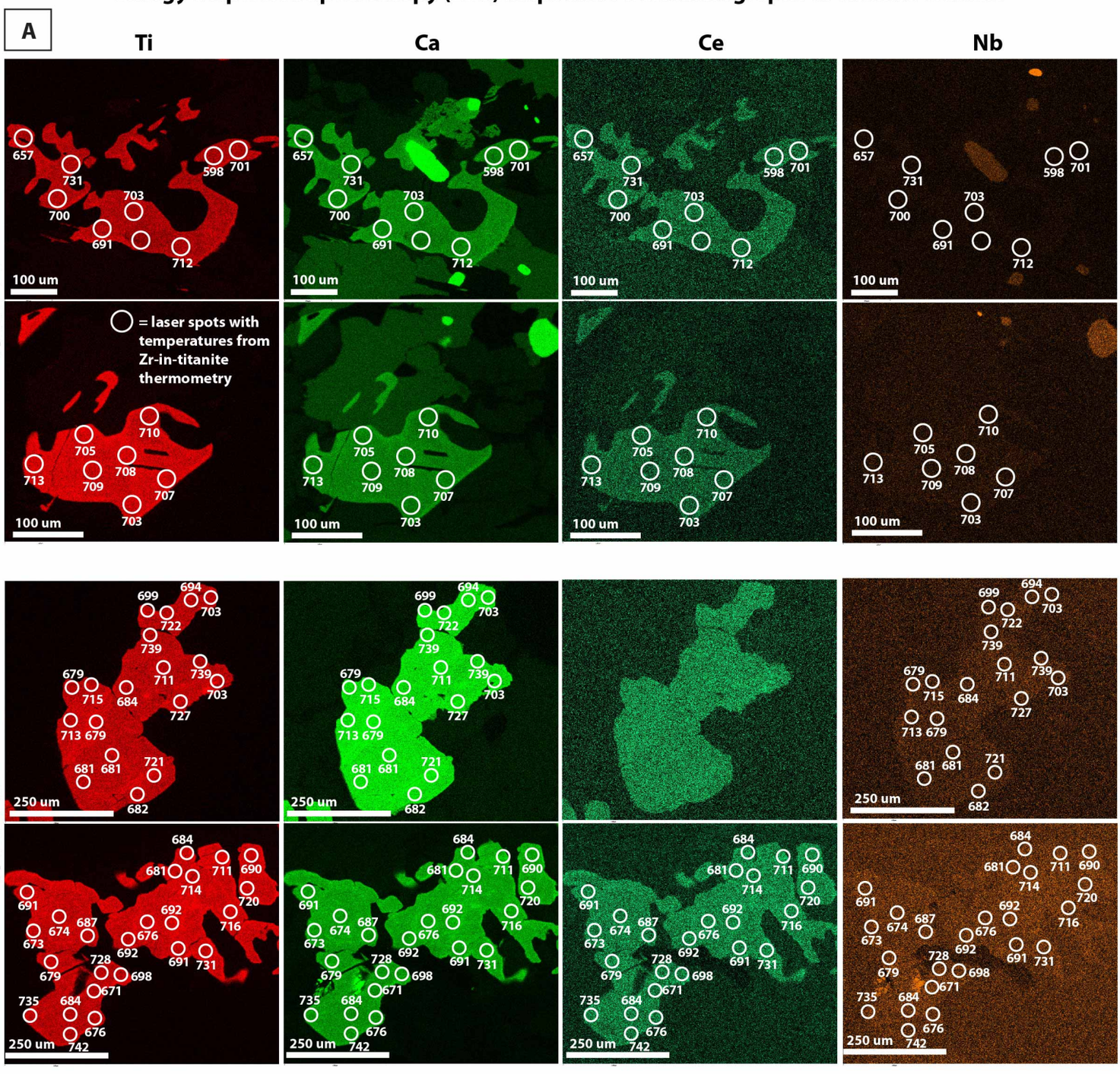

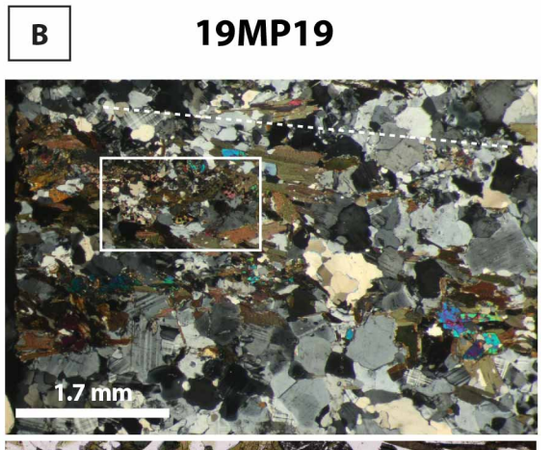

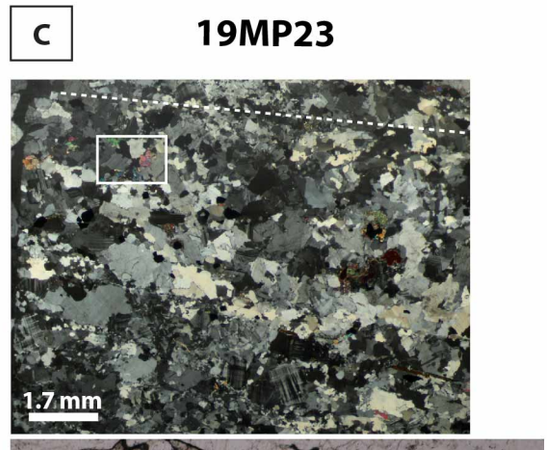

Figure SM2.

Misty Pluton Sample 19MT03

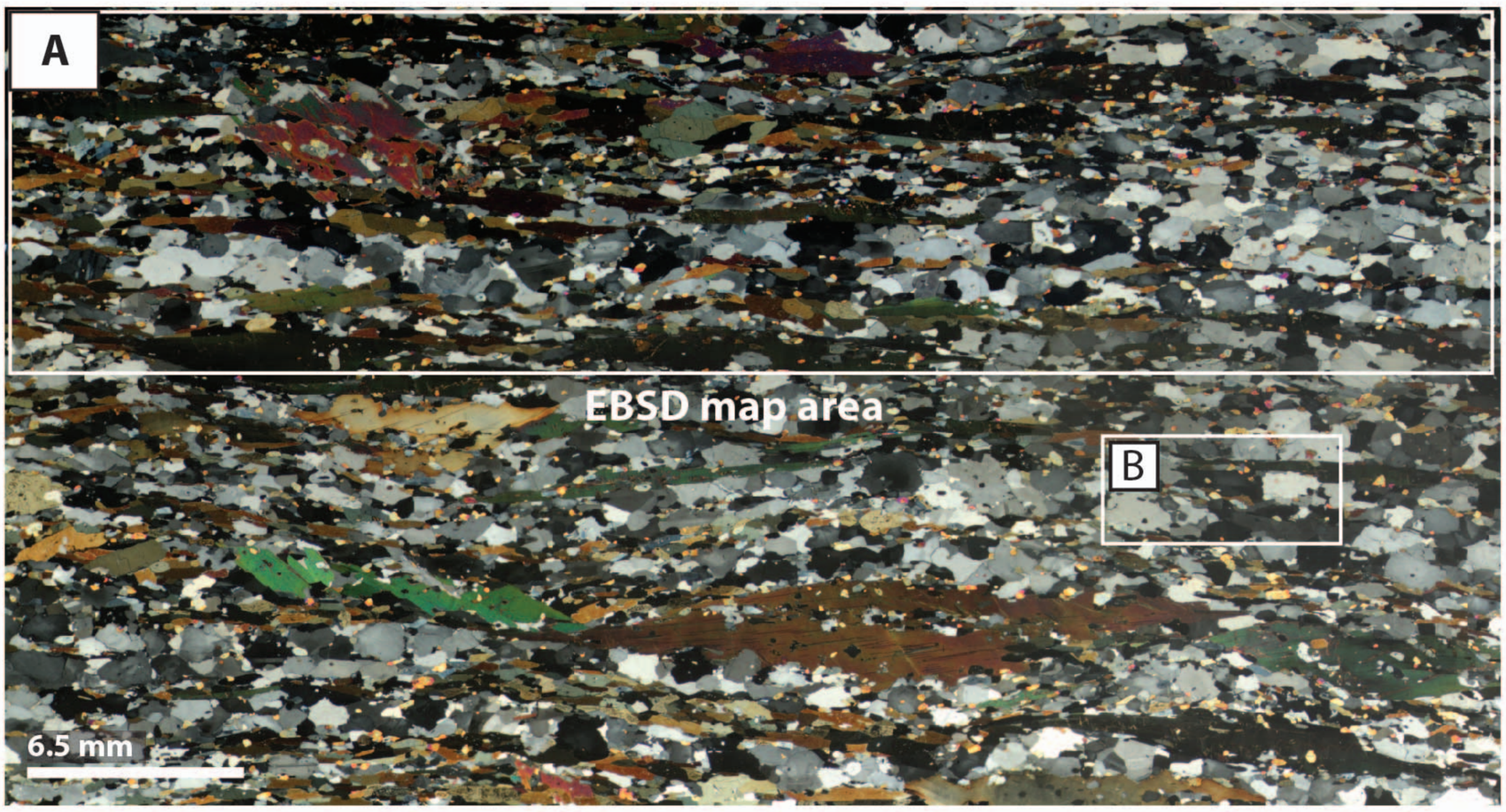

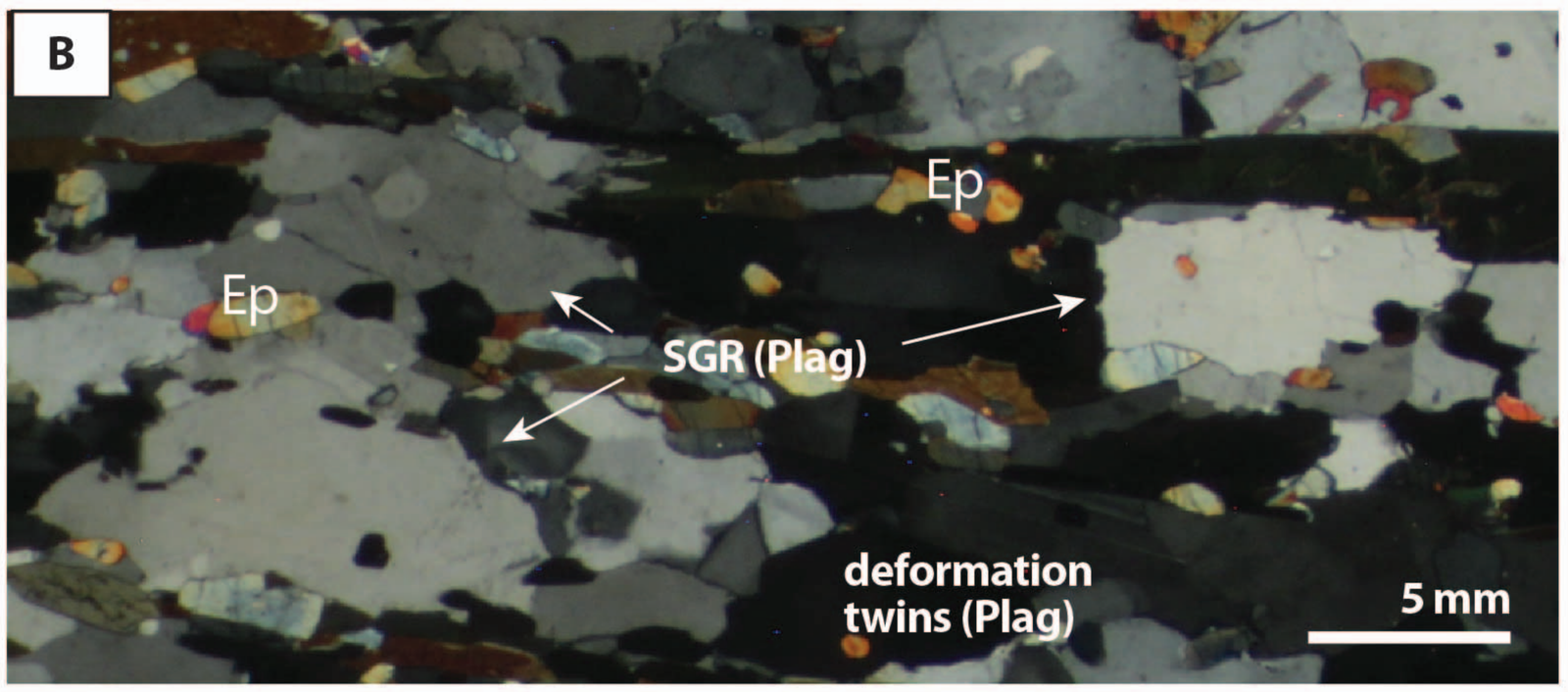

EBSD Phase Map Key

- 50% not indexed
- 25% plagioclase
- 5.2% quartz
- 0.95% biotite
- 17% hornblende
- 0.95% epidote
- 0.1% orthoclase
- 0% titanite
- 0.5% zircon
- 0.3% hydroxyapatite
- Grain Boundaries (>10° misorientatation)
- Dauphine Twin Boundaries (60° about (0001))

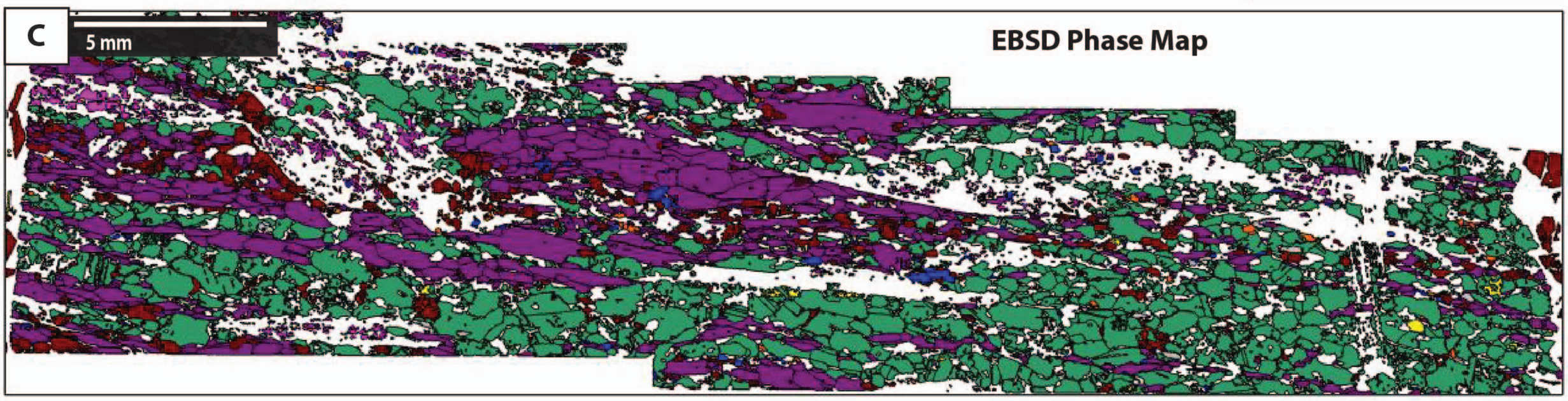

Figure SM3.

Misty Pluton Sample 19MT13

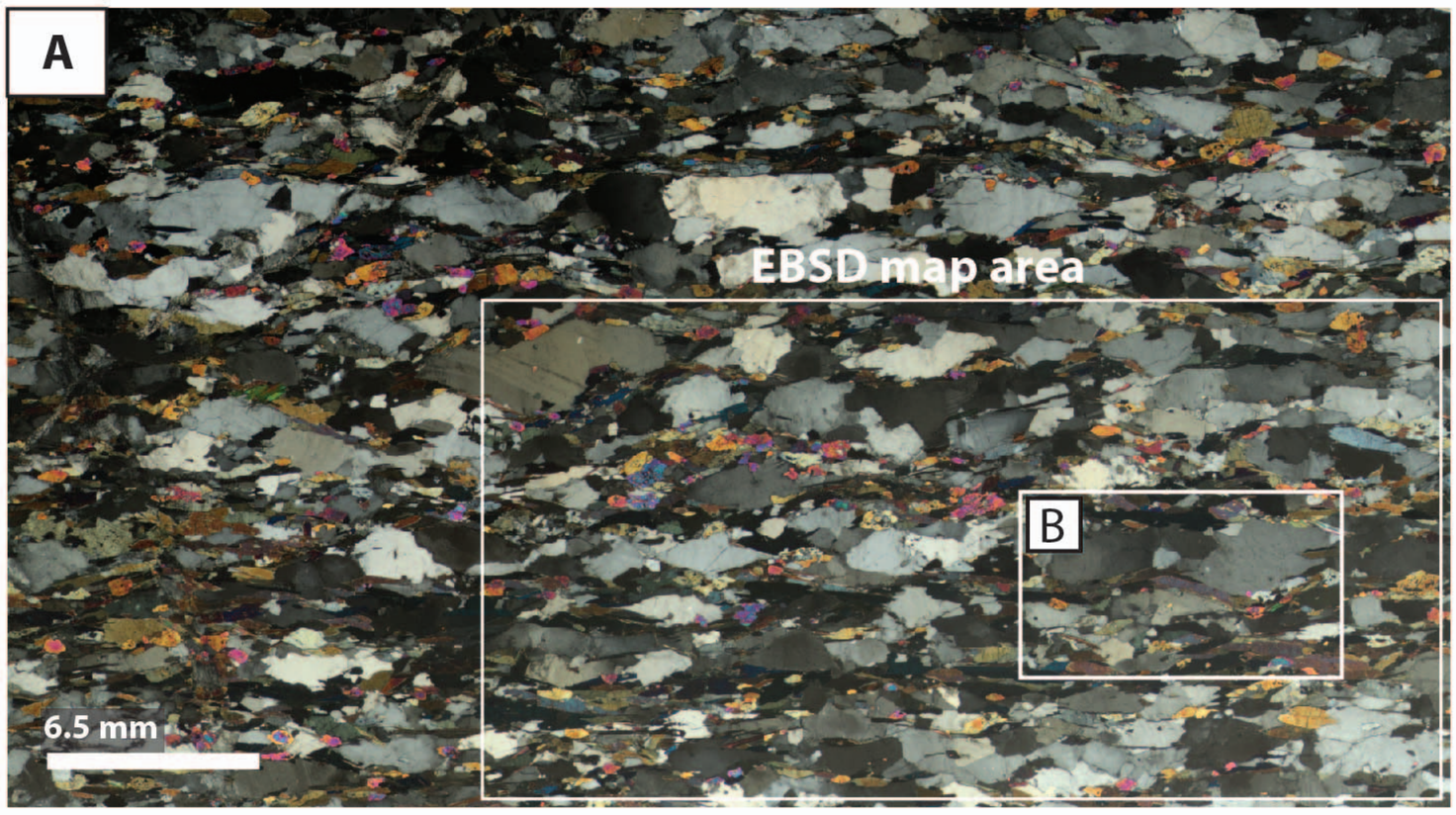

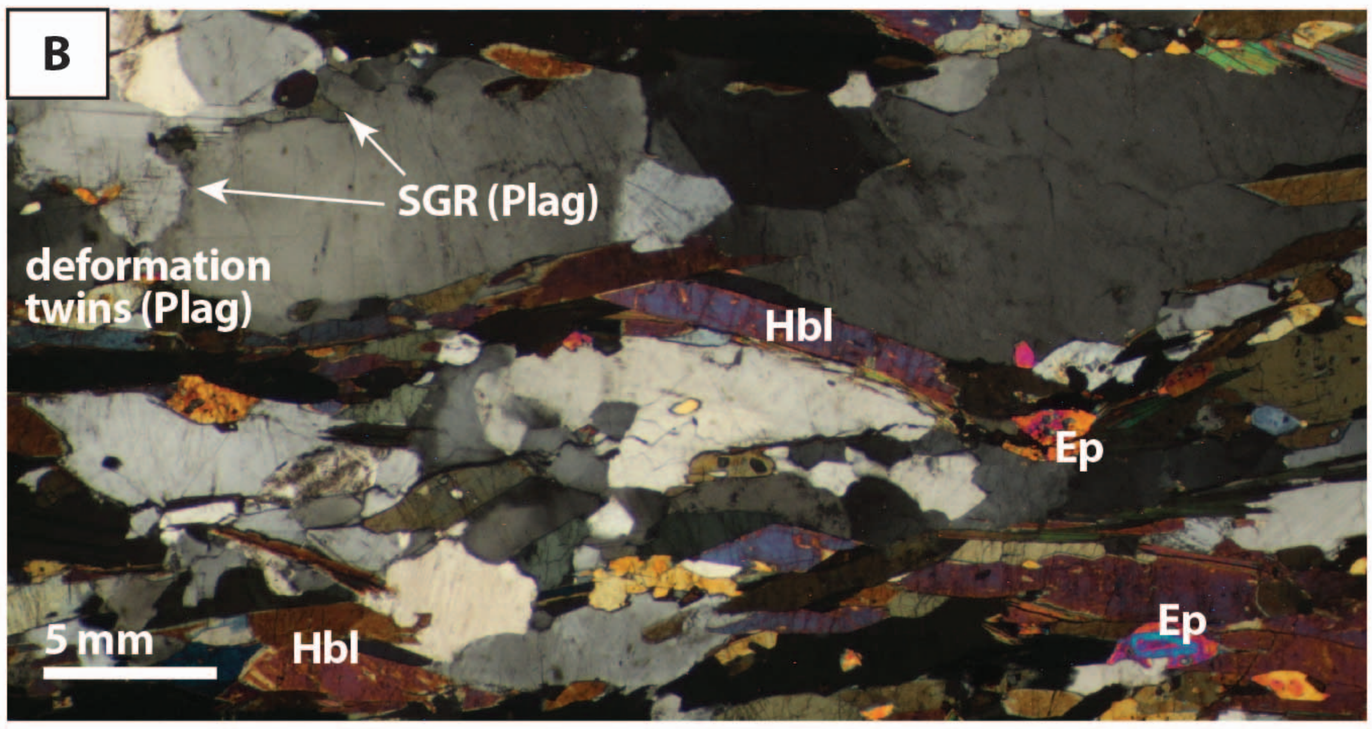

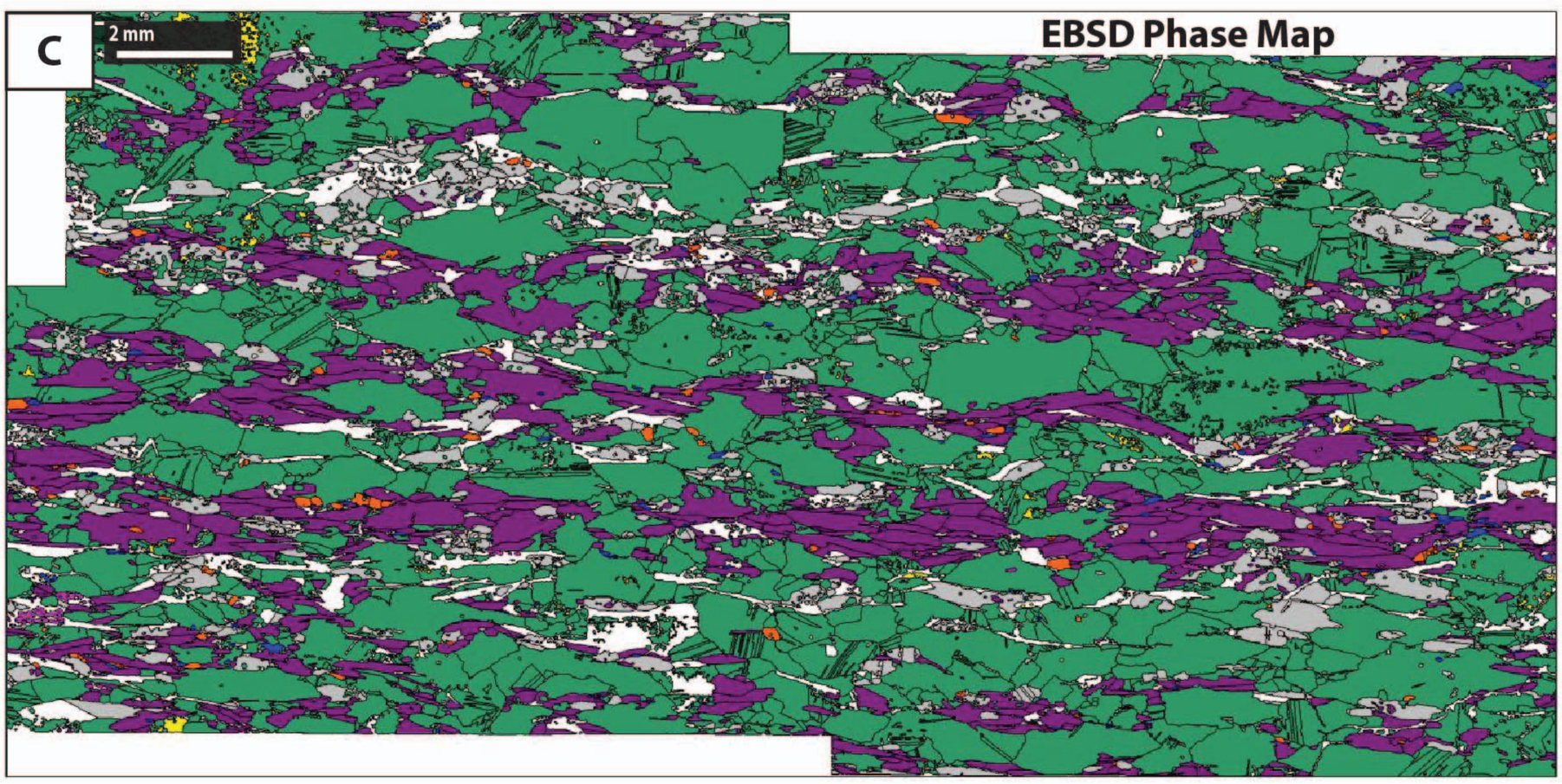

EBSD Phase Map Key

17%	not indexed
54%	plagioclase
0%	quartz
0.1%	biotite
19%	hornblende
8.3%	epidote
0.4%	orthoclase
0%	titanite
0.4%	zircon
0.5%	hydroxyapatite

Grain Boundaries (>10° misorientatation)

Figure SM4.

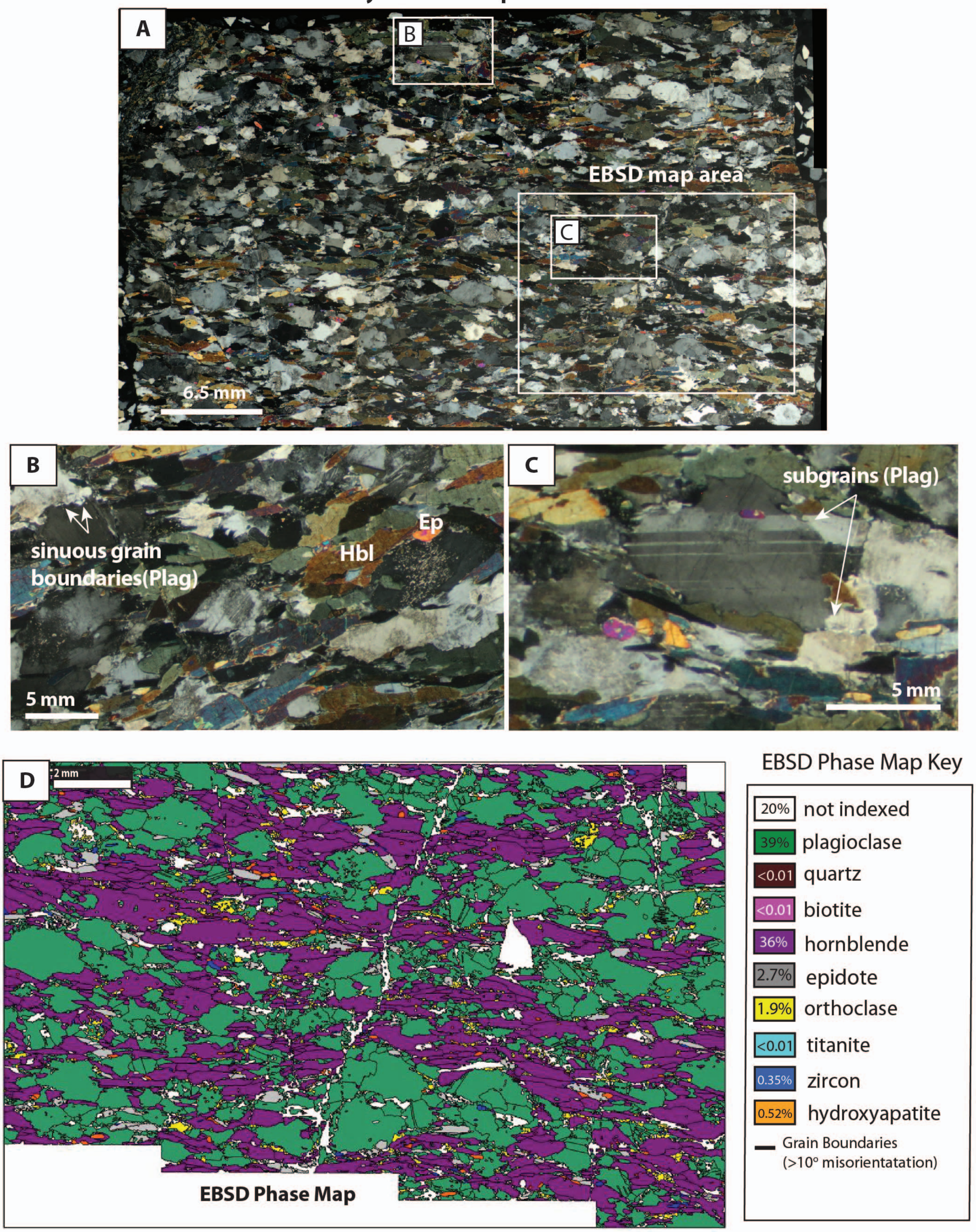
Misty Pluton Sample 19MT09
A
B
C
EBSD map area
6.5 mm
B
sinuous grain boundaries(Plag)
Hbl
Ep
5 mm
C
subgrains (Plag)
5 mm
D
2 mm
EBSD Phase Map
EBSD Phase Map Key
20% not indexed
39% plagioclase
<0.01 quartz
<0.01 biotite
36% hornblende
2.7% epidote
1.9% orthoclase
<0.01 titanite
0.35% zircon
0.52% hydroxyapatite
Grain Boundaries
(>10° misorientatation)

Figure SM5.

Large Pluton Sample 19MP19

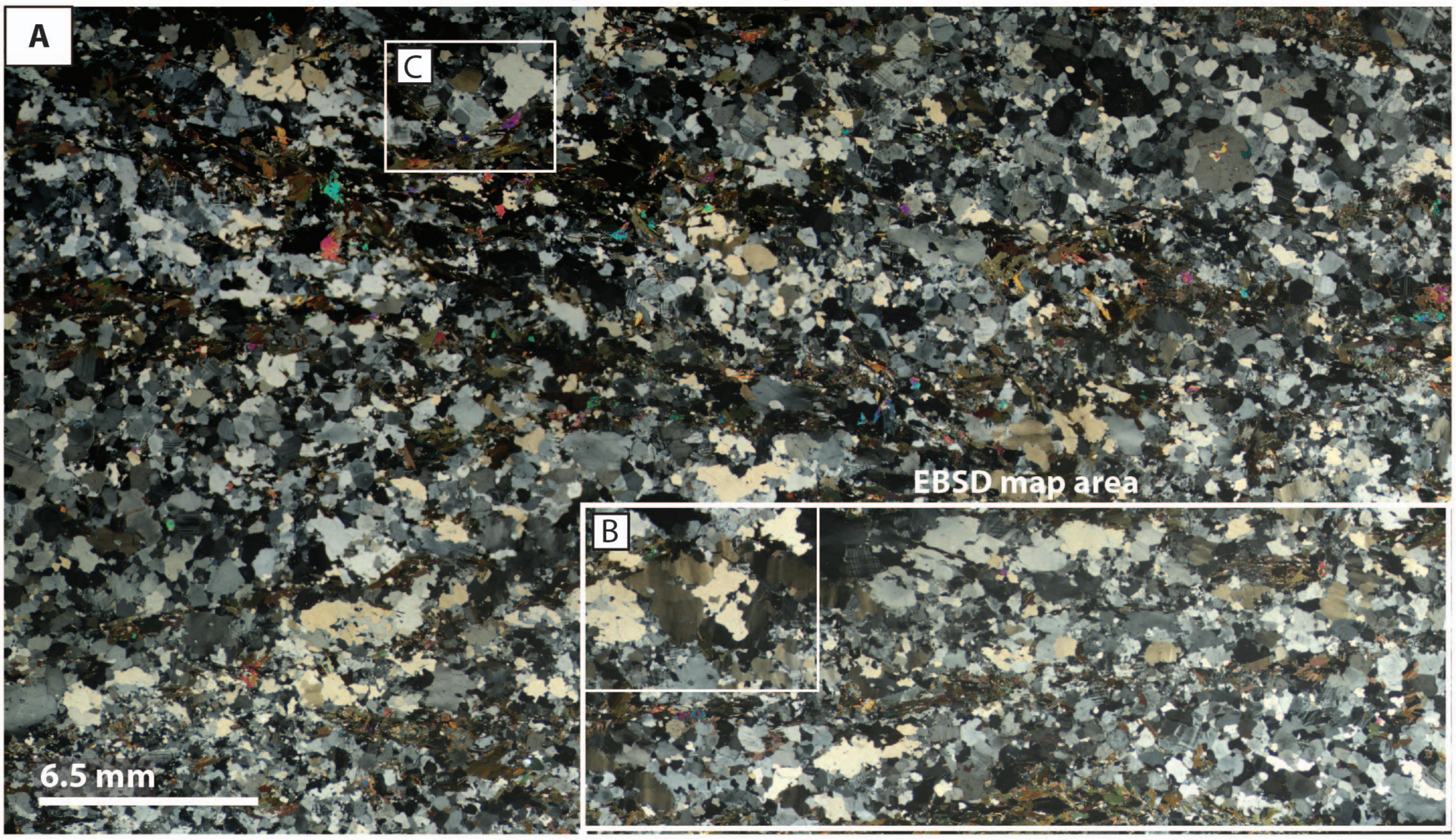

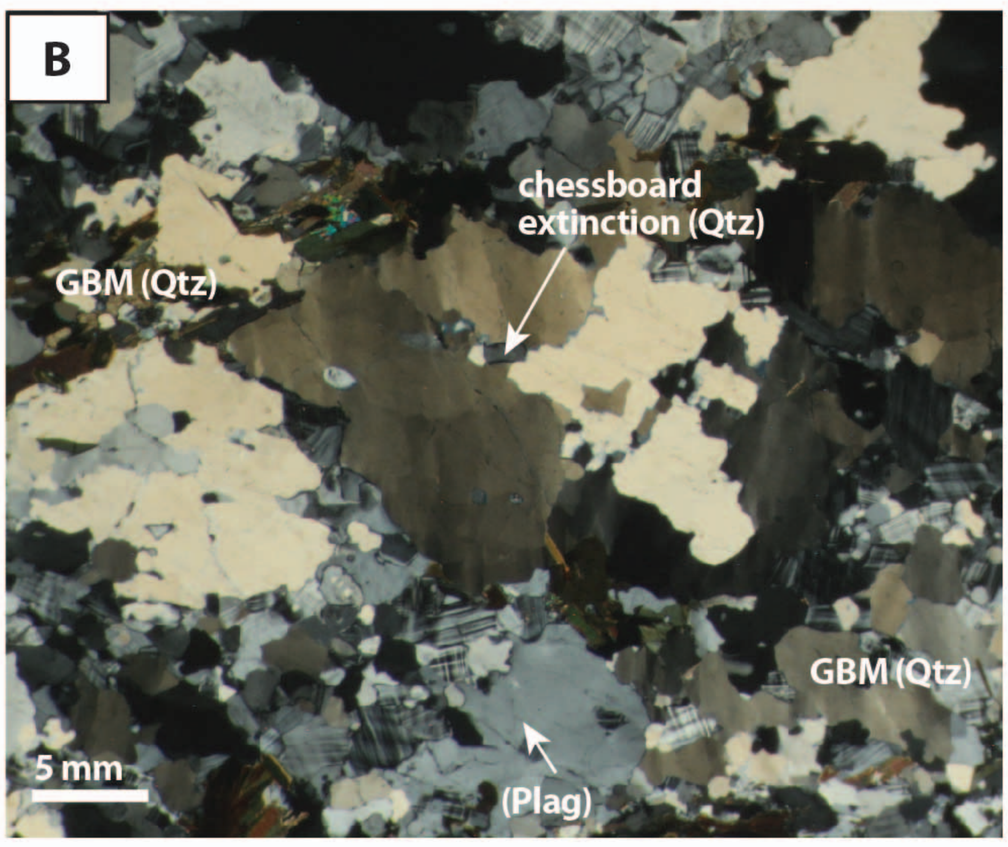

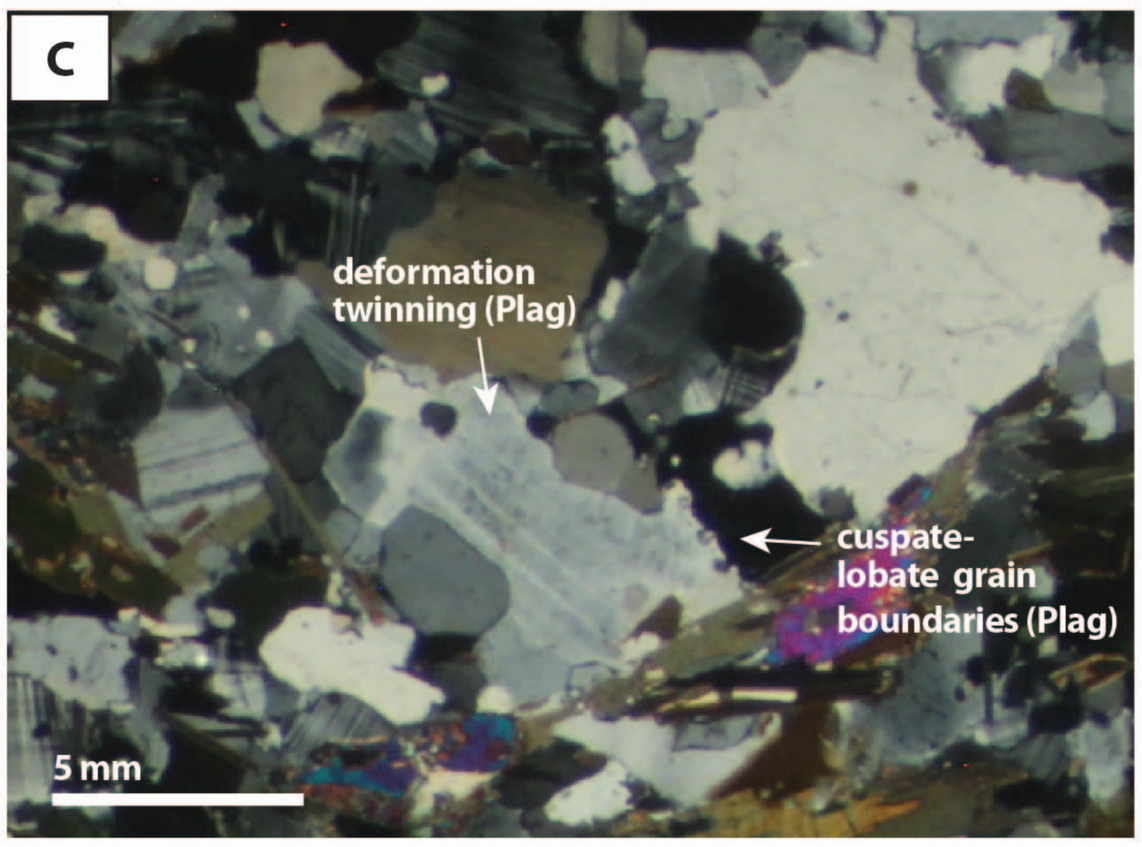

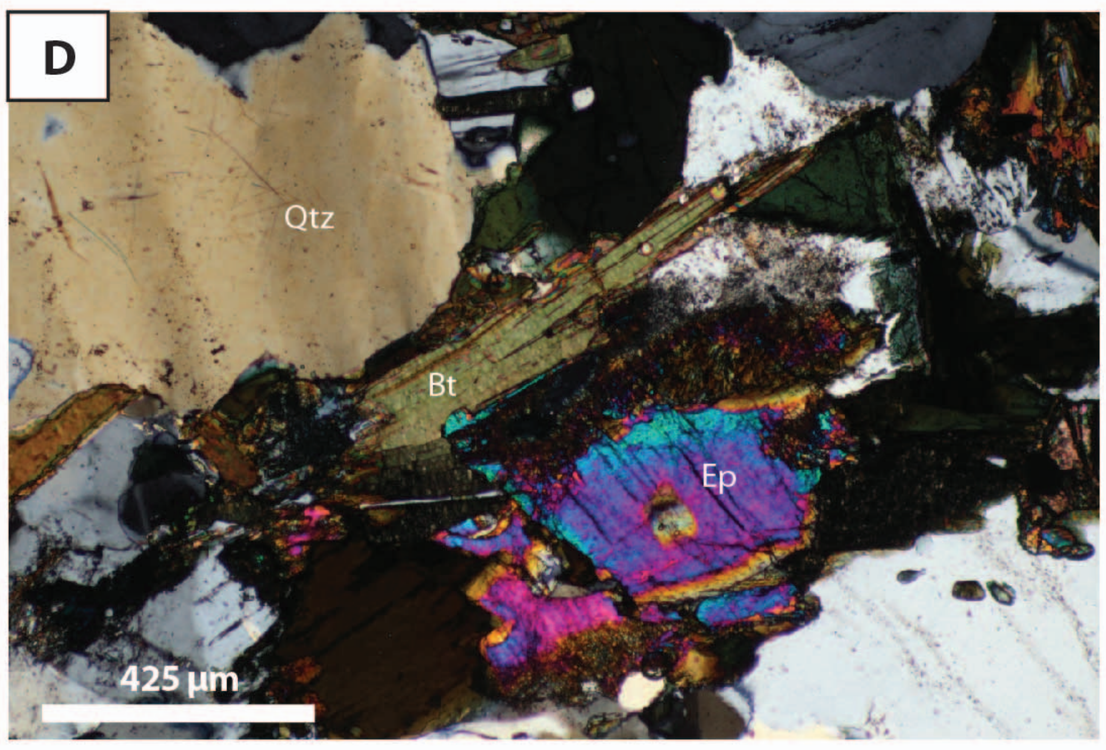

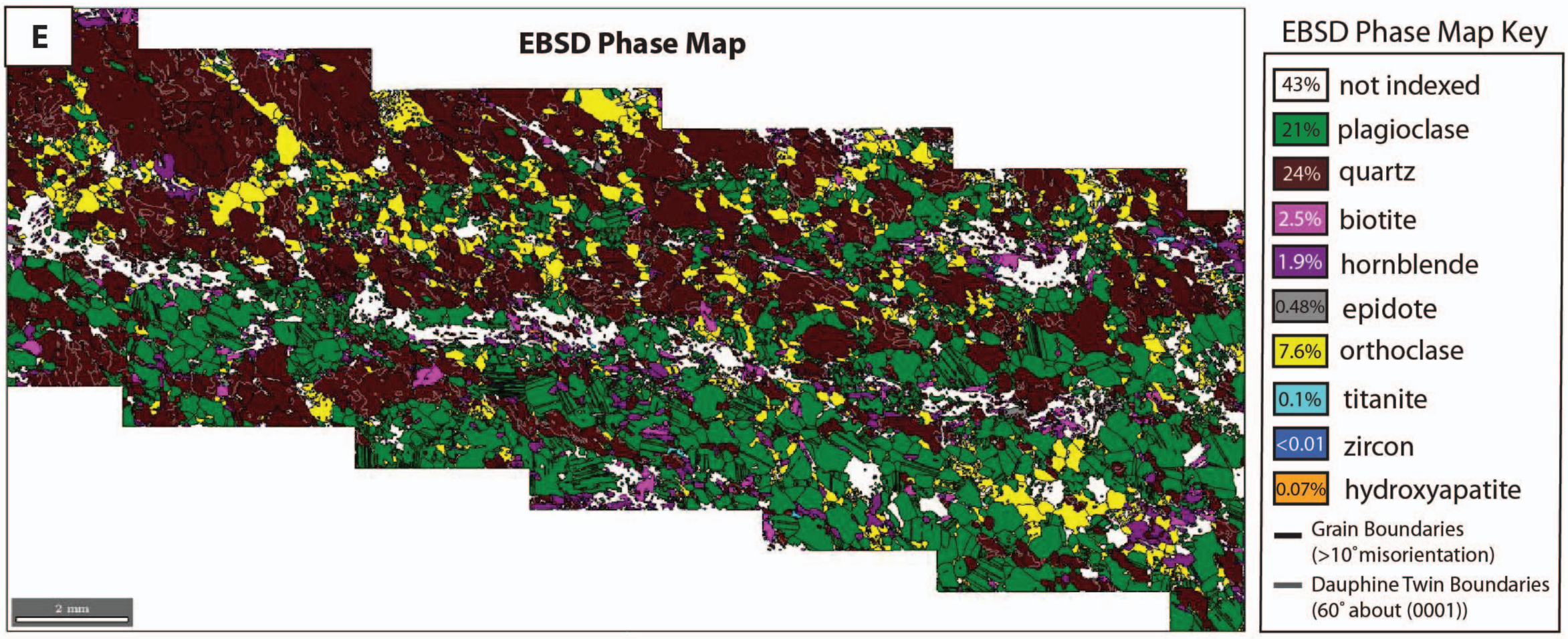

Figure SM6.

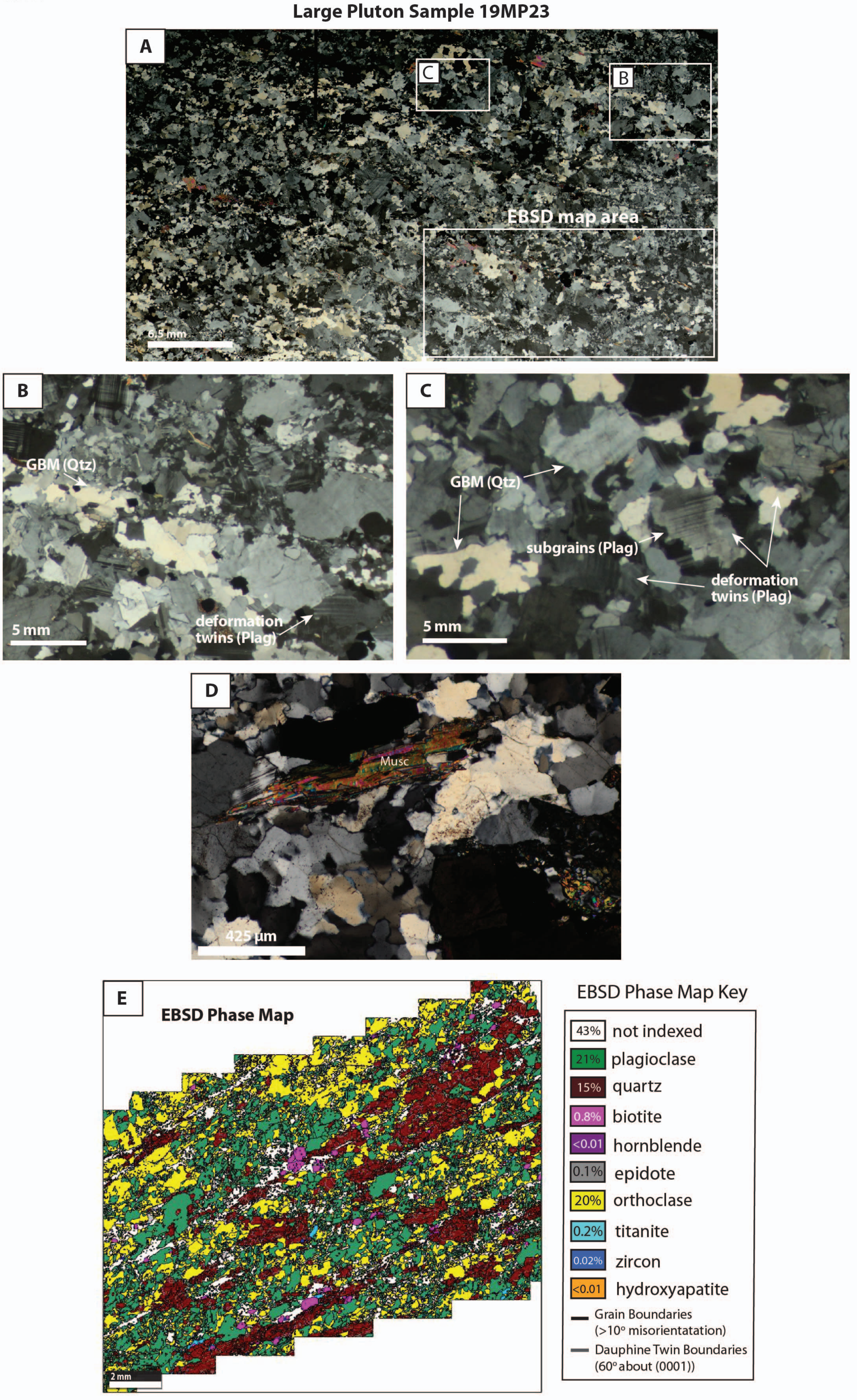
Large Pluton Sample 19MP23
A
C
B
EBSD map area
6.5 mm
B
GBM (Qtz)
deformation
twins (Plag)
5 mm
C
GBM (Qtz)
subgrains (Plag)
deformation
twins (Plag)
5 mm
D
Musc
425 µm
E
EBSD Phase Map
2 mm
EBSD Phase Map Key
43% not indexed
21% plagioclase
15% quartz
0.8% biotite
<0.01 hornblende
0.1% epidote
20% orthoclase
0.2% titanite
0.02% zircon
<0.01 hydroxyapatite
Grain Boundaries
(>10° misorientatation)
Dauphine Twin Boundaries
(60° about (0001))